

Clinicopathologic and molecular characteristics of neuroendocrine carcinomas of the gallbladder

Hui Tang^{1*}, Xiaojun Jiang^{1*}, Lili Zhu^{1*}, Liming Xu¹, Xiaoxi Wang¹, Hong Li², Feifei Gao³, Xinxin Liu⁴, Chuanli Ren⁵ and Yan Zhao⁶

¹Department of Pathology, ²Department of Hepatobiliary and Pancreatic Surgery, ³Department of Radiology, the First Affiliated Hospital, Zhejiang University School of Medicine, Hangzhou, Zhejiang, ⁴Department of General Surgery, Jiangsu Province Hospital of Chinese Medicine, Affiliated Hospital of Nanjing University of Chinese Medicine, Nanjing, ⁵Department of Laboratory Medicine and ⁶Medical Research Center, Northern Jiangsu People's Hospital, Northern Jiangsu People's Hospital Affiliated to Yangzhou University, Yangzhou, Jiangsu, China

*These authors contributed equally to this work

Summary. Gallbladder neuroendocrine carcinomas (GB-NECs) are a rare subtype of malignant gallbladder cancer (GBC). The genetic and molecular characteristics of GB-NECs are rarely reported. This study aims to assess the frequency of microsatellite instability (MSI) in GB-NECs and characterize their clinicopathologic and molecular features in comparison with gallbladder adenocarcinomas (GB-ADCs). Data from six patients with primary GB-NECs and 13 with GB-ADCs were collected and reevaluated. MSI assay, immunohistochemistry for mismatch repair proteins (MLH1, MSH2, MSH6, and PMS2), comprehensive genomic profiling (CGP) via next-generation sequencing (NGS), and evaluation of tumor mutation burden (TMB) were conducted on these samples. The six GB-NEC cases were all female, with a mean age of 62.0±9.2 years. Of these, two cases were diagnosed as large cell neuroendocrine carcinomas (LCNECs), while the remaining four were small cell neuroendocrine carcinomas (SCNECs). Microsatellite states observed in both GB-NECs and GB-ADCs were consistently microsatellite stable (MSS). Notably, *TP53* (100%, 6/6) and *RBI* (100%, 6/6) exhibited the highest mutation frequency in GB-NECs, followed by *SMAD4* (50%, 3/6), *GNAS* (50%, 3/6), and *RICTOR* (33%, 2/6), with *RBI*, *GNAS*, and *RICTOR* specifically present in GB-NECs. Immunohistochemical (IHC) assays of p53 and Rb in the six GB-NECs were highly consistent with genetic mutations detected by targeted NGS. Moreover, no statistical difference was observed in TMB between GB-NECs and GB-ADCs ($p=0.864$). Although overall

survival in GB-NEC patients tended to be worse than in GB-ADC patients, this difference did not reach statistical significance ($p=0.119$). This study has identified the microsatellite states and molecular mutation features of GB-NECs, suggesting that co-mutations in *TP53* and *RBI* may signify a neuroendocrine inclination in GB-NECs. The IHC assay provides an effective complement to targeted NGS for determining the functional status of p53 and Rb in clinical practice.

Key words: Gallbladder cancer, Neuroendocrine carcinoma, Adenocarcinoma, Microsatellite instability, Comprehensive genomic profiling

Introduction

Gallbladder cancers (GBCs) are rare digestive system malignancies, exhibiting a worldwide incidence of 1.2% and a mortality rate of 1.7% (Bray et al., 2018). Several predisposing factors, including chronic inflammation, genetic traits, gender differences, and developmental dysplasia, contribute to the distinct nature of this cancer (Hundal and Shaffer, 2014). Among GBCs, Gallbladder Adenocarcinomas (GB-ADCs) represent the predominant histological type, accounting for roughly 90% of cases (Roa et al., 2021).

Neuroendocrine neoplasms (NENs) originating from neuroendocrine cells are infrequent, primarily occurring in the digestive and respiratory systems (Gustafsson et al., 2008; La Rosa and Ucella, 2021). According to the 2022 WHO classification of endocrine and neuroendocrine tumors (Rindi et al., 2022), NENs are divided into well-differentiated neuroendocrine tumors (NETs), poorly differentiated neuroendocrine

Corresponding Author: Yan Zhao, 98 Nantong West Road, Guanglin District, Yangzhou, Jiangsu Province, 225001, China. e-mail: zhaoyan1982@foxmail.com

www.hh.um.es. DOI: 10.14670/HH-18-788



carcinomas (NECs), and Mixed neuroendocrine-non-neuroendocrine neoplasms (MiNENs), which are generally composed of adenocarcinoma and neuroendocrine carcinoma ($\geq 30\%$ of tumor burden). NECs further subdivide into small cell types (SCNECs) or large cell types (LCNECs) based on morphological features. Gallbladder neuroendocrine carcinomas (GB-NECs) are exceedingly rare and highly malignant, constituting only 0.5% of all NENs and 2.1% of GBCs (Yao et al., 2008). Owing to the absence of specific clinical manifestations and typical imaging features in GB-NECs, it is difficult to distinguish GB-NECs from GB-ADCs without pathological diagnosis. Unfortunately, GB-NECs are typically diagnosed at advanced stages, resulting in unsatisfactory outcomes and a poor prognosis.

Microsatellite instability (MSI) has been observed in intestinal and gastric neuroendocrine carcinomas (Sahnane et al., 2015). However, microsatellite states in GB-NECs have been rarely reported. Moreover, owing to its low incidence, the molecular characteristics of GB-NECs remain largely unknown. Molecular disparities between GB-NECs and GB-ADCs have not been clearly recognized. In this study, we reported and analyzed the histopathological and molecular characteristics of six poorly differentiated GB-NEC cases. Additionally, we provided detailed insights into the microsatellite states and comprehensive genomic profiles (CGP) of these rare cases of GB-NECs alongside 13 GB-ADC cases. Identifying gene mutation disparities between GB-NECs and GB-ADCs may aid in identifying specific molecular pathological diagnostic biomarkers of GB-NECs.

Materials and methods

Patients and study design

This retrospective study examined six patients with GB-NECs admitted to the First Affiliated Hospital, Zhejiang University School of Medicine between January 2018, and January 2023. Pathological diagnoses were confirmed by two expert pathologists using four postoperative resection specimens and two biopsy specimens. Thirteen age-matched patients with GB-ADCs who underwent surgical resection and received

confirmed pathological diagnoses were randomly selected for comparison. Detailed clinical information for each patient, including sex, age, physical examinations, presence of gallbladder stones, surgical treatment, pathologic diagnosis, serum tumor markers, and prognosis, was recorded. All samples were analyzed using an MSI assay and comprehensive genomic profiling through NGS sequencing. The Ethics Committee of the First Affiliated Hospital, Zhejiang University School of Medicine approved this study (No. 2023-0579). Patient consent was waived due to the retrospective study using previous medical records.

Morphologic assessment

All tissue samples were fixed in 4% paraformaldehyde, embedded in paraffin wax, and sectioned (thickness, 3 μm). Paraffin sections were stained with hematoxylin-eosin (H&E) for morphological examinations. Expert pathologists evaluated histological features according to the WHO Classification of Endocrine and Neuroendocrine Tumors (2022), including neuroendocrine cytologic subtype (small or large cell), tumor grade, exocrine component type (adenomas, adenocarcinomas, squamous cell carcinomas), vascular and perineural invasion, presence of necrosis, mitotic count per 2 square mm, bile duct infiltration, liver or pancreas tissue invasion, resected margins, and local lymph node metastases. TNM stage was assigned according to the 8th American Joint Committee on Cancer (AJCC) guidelines for gallbladder cancer (Byrd et al., 2017).

Immunohistochemical staining

Consecutive tissue sections (3 μm) underwent dewaxing, rehydration, epitope retrieval, primary antibody incubation, and detection using the Leica Bond polymer refine detection kit (Leica, Germany) or Ventana® Ultraview universal DAB detection kit (Roche, Switzerland), following the primary antibody's instruction manual. Detailed antibody information is listed in Table 1. The Ki67 proliferative index was calculated as Ki-67+ staining (%): $\text{Ki-67+ tumor cells} / (\text{Ki-67+ tumor cells} + \text{Ki-67- tumor cells}) \times 100$. A total

Table 1. Antibody list used in IHC.

Antibodies	Catalog no.	Source	MAb/RAb	Dilution
Anti-Syn	ZA-0506	ZSGB-BIO, Beijing	M	1:300 for IHC/IF
Anti-CD56	M-0148	Shangai Long Island Biotec. Co.	M	1:300 for IHC/IF
Anti-CgA	M-0202	Shangai Long Island Biotec. Co.	M	1:500 for IHC/IF
Anti-Ki-67	MIB-1	DAKO, Denmark	M	1:1000 for IHC/IF
Anti-MSH2	BPM6143	Biolyinx, Hangzhou	M	1:200 for IHC/IF
Anti-MSH6	ZA-0541	ZSGB-BIO, Beijing	R	1:200 for IHC/IF
Anti-MLH1	ZM-0154	ZSGB-BIO, Beijing	M	1:100 for IHC/IF
Anti-PMS2	ZA-0542	ZSGB-BIO, Beijing	R	1:50 for IHC/IF
Anti-p53	DO-7	Enzo, American	M	1:1000 for IHC/IF
Anti-Rb	AM0207	Talent Biomedical Technology Co., Ltd, Xiamen	M	1:1000 for IHC/IF

Molecular characteristics of GB-NECs

of 2000 tumor cells in areas with the highest immunostaining were counted. MSH6, MSH2, MLH1, and PMS2 were used to examine the expression of mismatch repair (MMR) proteins. IHC staining of Syn, CgA, CD56, Ki-67, and p53 used known positive tissue samples as positive controls, MSH6, MSH2, MLH1, PMS2, and Rb used known negative tissue samples as negative controls. Non-malignant tissue was used as an internal control for each sample. Two independent pathologists evaluated the IHC slides based on the intensity and extent of the staining observed under a microscope.

Microsatellite instability assay by PCR

Genomic DNA from paired tumor-normal tissue paraffin sections was extracted using a commercial DNA FFPE tissue extraction kit. MSI analysis was performed using an MSI detection kit (SINOMD gene, China) on the ABI 3500 Genetic Analyzer (ABI, USA), evaluating a panel of five monomorphic mononucleotide repeat sequences (BAT25, BAT26, NR-21, NR-22, and NR-24). Microsatellite instability at two or more loci was interpreted as MSI-high (MSI-H); instability at a single locus was MSI-low (MSI-L); no instability at any locus was interpreted as microsatellite stable (MSS). Both normal and tumor tissue from each patient were assessed.

Comprehensive genomic profiling (CGP) sequencing and tumor mutational burden (TMB) estimation

Genomic DNA was extracted from the FFPE tumor samples of GB-NECs and GB-ADCs using a commercial DNA FFPE tissue extraction kit according to the manufacturer's protocol (Concertbio Inc., China). Libraries were constructed with fragmented DNA, purified, end-repaired, ligated with indexed pair-end adaptors, and amplified by polymerase chain reaction (PCR). The quality-controlled DNA libraries were sequenced using OncoScreen[®] Plus (Burning Rock Dx Inc., China) or GENESEQ PRIME[®] (Geneseq Technology Inc., China) panels on the Illumine MiseqDx/NextSeq platform, covering 520 and 425 cancer-related genes, respectively. Although the two CGP panels covered different genes, the most commonly known cancer-related genes were included. Parallel sequencing was performed on paired peripheral blood leukocytes to filter germline variants. Sequencing results were mapped to the human genome reference GRCh37/hg19. A variety of mutations, including single-nucleotide variants (SNVs), small insertion-deletion, and copy number variations (CNV), were detected. Mutation types were categorized as missense, nonsense, frameshift, or splice site mutations, initiator codon loss, copy number loss, copy number amplification, and mutations in non-coding regions. Pathway enrichment analysis was conducted using PANTHER18.0 (<https://www.pantherdb.org/>).

TMB, representing the number of somatic mutations

per million bases in the genome, was estimated based on the total number of non-silent mutations within the panel's detection range. MSI status was determined by evaluating microsatellite sites' length distribution through an MSI algorithm using NGS Sequencing data, as previously reported. (Zhu et al., 2018)

Statistical analysis

Continuous parameter associations were assessed using independent sample Student's t-tests, while categorical data comparisons were made using the Chi-square test or Fisher's exact test. Patient survival was evaluated by the Kaplan-Meier method and statistically tested with the log-rank test. *p*-values < 0.05 were considered statistically significant. GraphPad Prism V8.0 software was used for these analyses and visualizations (San Diego, CA, USA).

Results

Clinical characteristics of GB-NEC and GB-ADC patients

All six GB-NEC patients were female, with ages ranging from 52 to 73 years and a median age of 62.0 years. Among these cases, four (4/6) experienced upper abdominal pain, and five (5/6) presented with complications related to gallbladder stones. Jaundice was observed in only one case (1/6). Imaging assessments via computed tomography (CT) or magnetic resonance imaging (MRI) led to a presumptive diagnosis of gallbladder carcinoma in all examined patients. Laboratory findings indicated elevated CA199, CA125, and CA153 levels in two patients (33.3%), with one patient exhibiting increased ferritin levels (16.7%). In contrast, CEA levels were within the normal range for all GB-NEC patients, while four GB-ADC patients (30.8%) exhibited elevated CEA levels. However, there was no significant difference noted in these serum tumor markers between the two groups.

Four GB-NEC patients underwent radical cholecystectomy, accompanied by synchronous hepatic segmental or extrahepatic bile duct resection based on individual patient conditions, followed by postoperative chemotherapy. Conversely, two GB-NEC patients with unresectable lesions solely underwent biopsy procedures and subsequently received chemotherapy. Detailed clinical characteristics of GB-NEC and well-matched GB-ADC patients are summarized in Table 2.

Pathologic and immunohistochemical features of GB-NEC patients

Two cases were situated at the fundus, two at the body, and two at the neck of the gallbladder (Table 3). The resected GB-NECs exhibited diameters ranging from 2.5 to 7.5 cm, with a median diameter of 4.55 cm. Concerning AJCC staging, two cases were classified as stage IIIA, one case as stage IIIB, while three cases were categorized as stage IVB. Lymph node metastasis was

Molecular characteristics of GB-NECs

identified in one case of LCNEC and two cases of SCNEC. Distant metastasis to the liver was detected in three cases of SCNECs. Vascular and perineural invasion were observed in all cases (4/4) (Table 3).

Morphological assessment revealed that two cases were LCNECs characterized by deeply stained,

vesicular-like nuclei, and abundant cytoplasm (Fig. 1, cases 1-2). Four cases were SCNECs, displaying small to medium-sized cells with scant cytoplasm and hyperchromatic nuclei with indistinct nucleoli (Fig. 1, cases 3-6). Mitoses were more frequently observed in

Table 2. Clinical characteristics of GB-NEC and GB-ADC patients.

Variables	GB-NECs (n=6)	GB-ADCs (N=13)	<i>p</i> value
<i>Age (years)</i>			0.895
Mean±SD	62.0±9.2	62.8±12.5	
Range	52-73	36-77	
<i>Sex</i>			0.225
Male	0	4	
Female	6	9	
<i>Abdominal pain</i>			>0.999
Yes	4	8	
No	2	5	
<i>Gallbladder stone</i>			>0.999
Yes	5	10	
No	1	3	
<i>Jaundice</i>			>0.999
Yes	1	4	
No	5	9	
<i>Laboratory Test</i>			
NLR (> 4)	5 (83.3%)	10 (76.9%)	>0.999
CEA (> 5ng/ml)	0 (0%)	4 (30.8%)	0.255
CA199 (> 37U/ml)	2 (33.3%)	9 (75.0%, n=12)	0.141
CA125 (> 35U/ml)	2 (33.3%)	2 (18.2%, n=11)	0.584
AFP (> 20ng/ml)	0 (0%)	1 (0.08%)	>0.999
Ferritin (> 323ng/ml)	1 (16.7%)	5 (45.5%, n=11)	0.333
CA153 (> 20U/ml)	2 (40.0%, n=5)	0 (0%, n=7)	0.151
<i>Surgical treatment</i>			
Radical resection ^a	4 (n=4)	12	
Extensive radical resection ^b	0 (n=4)	1	
<i>Receipt of chemotherapy</i>			
Yes	6	13	
No	0	0	
<i>Follow-up (months)</i>			
Range time	7-26	2-46 (n=7)	
Median time	16	31 (n=7)	

^a: Radical resection: patients received synchronous hepatic segmental or extrahepatic bile duct resection according to the conditions of patients. ^b: Extensive radical resection: patients underwent partial liver resection, colon resection, and pancreaticoduodenectomy.

Table 3. Pathologic features of GB-NEC and GB-ADC patients.

Variables	GB-NECs (n=6)	GB-ADCs (n=13)	<i>p</i> value
<i>Primary tumor site</i>			0.850
Fundus	2	4	
Body	2	4	
Neck	2	5	
<i>Pathologic classification</i>			
GB-NECs large cell subtype	2 (33.3%)		
GB-NECs small cell subtype	4 (66.7%)		
Adenocarcinoma		13 (100%)	
<i>Pathologic grade</i>			
good differentiation		1 (7.7%)	
moderate differentiation		1 (7.7%)	
moderate-poor differentiation		9 (69.2%)	
poor differentiation	6 (100%)	2 (15.4%)	
<i>Tumor size</i>	4.65±1.88 ^a	3.18±1.12	0.068
<i>AJCC pathologic tumor stage</i>			0.441
Stage IIA	0 ^b	1	
Stage IIB	0 ^b	3	
Stage IIIA	2 ^b	5	
Stage IIIB	1 ^b	2	
Stage IVB	3 ^b	2	
<i>Tumor depth</i>			0.213
T2a	2 ^b	1	
T2b	0 ^b	3	
T3	4 ^b	9	
<i>Lymph node metastasis</i>			0.0886
N0	3 ^b	10	
N1	1 ^b	3	
N2	2 ^b	0	
<i>Distant metastasis</i>	3 (50%) ^b	2 (15.4%)	0.075
<i>Vascular invasion</i>	4 (100%) ^a	8 (61.5%)	0.261
<i>Perineural invasion</i>	4 (100%) ^a	6 (46.2%)	0.103
<i>Negative margin status</i>	4 (100%) ^a	13 (100%)	1.000

^a: n=4, four GB-NEC cases with surgical section were evaluated. ^b: n=6, four GB-NEC cases with surgery provided pathologic AJCC and TNM stagings, and the other two cases without surgery provided the clinical AJCC and TNM stagings.

Table 4. Immunohistochemical and MSI molecular characterization in GB-NEC patients.

Case No.	Histological subtype	Syn (100%)	CgA (50%)	CD56 (83.3%)	Ki-67 (%)	P53	RB1	MMR proteins				MSI by PCR
								MSH6	MSH2	MLH1	PMS2	
1	LCNEC	+	+	-	70	-	-	+	+	+	+	MSS
2	LCNEC	+	+ local	+	70	+*	-	+	+	+	+	MSS
3	SCNEC	+	+	+	90	+*	-	+	+	+	+	MSS
4	SCNEC;	+ weak	-	+	95	-	-	+	+	+	+	MSS
5	SCNEC	+	-	+	80	-	+ weak	+	+	+	+	MSS
6	SCNEC	+ weak	-	+ local	90	-	-	+	+	+	+	MSS

*: cytoplasmic expression pattern of the P53 protein; LCNEC: large cell neuroendocrine carcinoma; SCNEC: small cell neuroendocrine carcinoma; Syn: synaptophysin; CgA: chromogranin A; MMR: mismatch repair; MSI: microsatellite instability; MSS: microsatellite stability.

Molecular characteristics of GB-NECs

each sample.

IHC staining of synaptophysin (Syn), chromogranin A (CgA), and CD56 was employed to assess the neuroendocrine cell component. The positive rates for Syn, CgA, and CD56 were 100% (6/6), 50% (3/6), and 83.3% (5/6), respectively (Fig. 1, Table 4). The six NECs comprised poorly differentiated cells, demonstrating Ki67 proliferative indices ranging from 70% to 95% (Table 4).

MSI molecular characterization in GB-NEC and GB-ADC patients

To validate the microsatellite status, we analyzed the mononucleotide panel consisting of BAT-25, BAT-26, CAT-25, NR-24, and MONO-27. Each patient's tumor

tissue as well as its corresponding normal part underwent simultaneous analysis. All six GB-NEC cases exhibited MSS. Correspondingly, IHC expression of MMR proteins (MSH6, MSH2, MLH1, and PMS2) was positive in all GB-NEC patients (Table 4). The incidence of the MSI phenotype was also investigated in 13 GB-ADC patients. Similarly, mononucleotide MSI analysis of these patients revealed microsatellite stability, and intact IHC expression of MMR proteins was observed (Table 4).

Distinct genetic mutations between GB-NECs and GB-ADCs

CGP sequencing of tumor samples unveiled a spectrum of genetic mutations in both GB-NEC and GB-

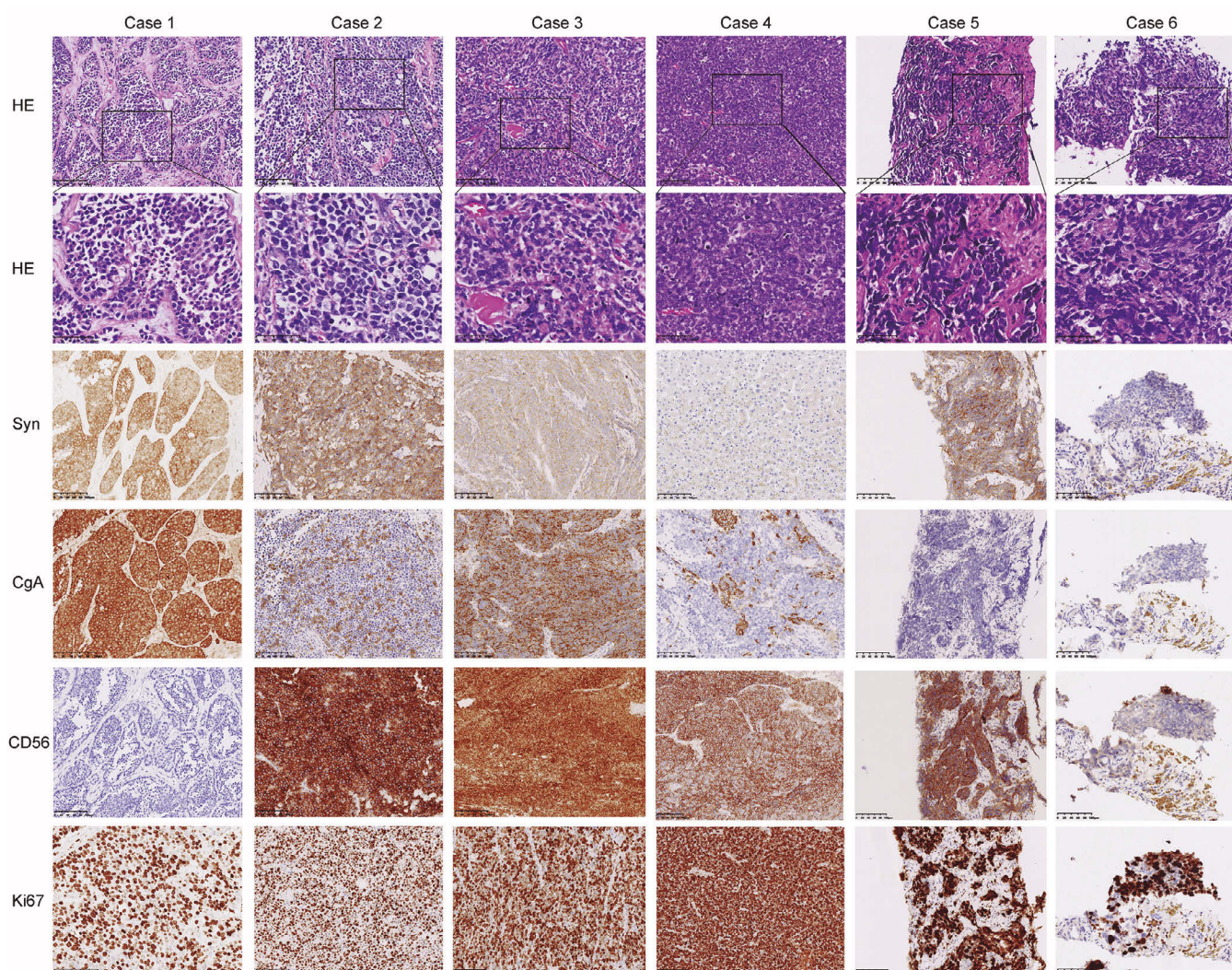


Fig. 1. Morphology and immunohistochemical profile of the 6 GB-NECs cases. Case 1: LCNEC, positive for Syn and CgA, negative for CD56, Ki67 proliferative index 70%. Case 2: LCNEC, positive for Syn and CD56, locally positive for CgA, Ki67 proliferative index 90%. Case 3: SCNEC, positive for Syn, CgA and CD56, Ki67 proliferative index 90%. Case 4: SCNEC, weakly positive for Syn, negative for CgA, positive for CD56, Ki67 proliferative index 70%. Case 5: SCNEC, positive for Syn and CD56, negative for CgA, Ki67 proliferative index 80%. Case 6: SCNEC, weakly positive for Syn, negative for CgA, locally positive for CD56, Ki67 proliferative index 90%. HE staining scale bar: 50um, IHC staining scale bar: 100 μ m.

Molecular characteristics of GB-NECs

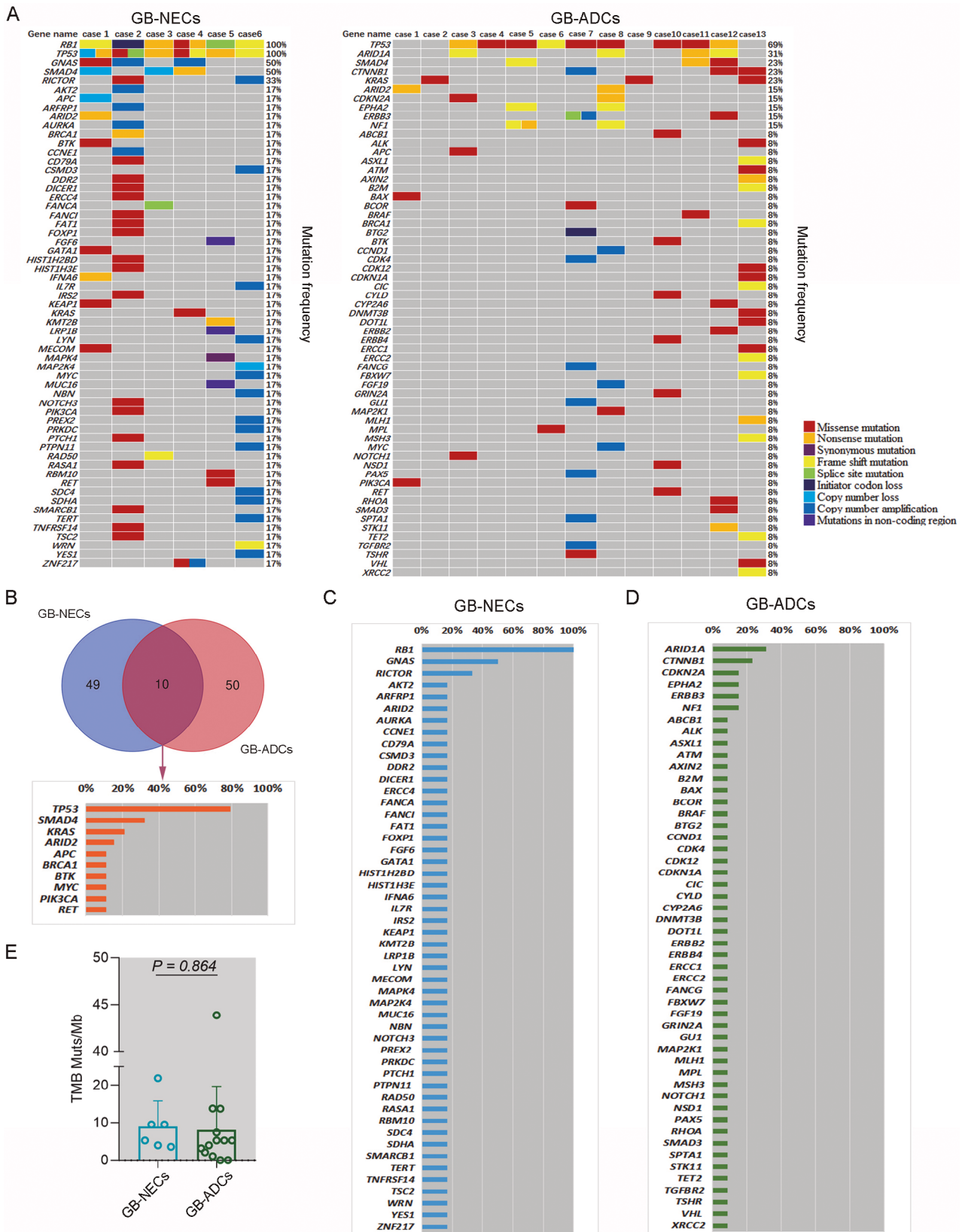


Fig. 2. Characteristics of genetic mutations in GB-NECs and GB-ADCs. **A.** Mutated gene names, mutation types, frequency and distribution in six GB-NECs and 13 GB-ADCs cases. **B.** Overlap of mutated genes detected in both GB-NECs and GB-ADCs (upper), the frequency of overlapping mutated genes in all cases (lower). **C.** Mutated gene names and frequency specially observed in GB-NECs. **D.** Mutated gene names and frequency specially observed in GB-ADCs. **E.** Comparison of tumor mutational burdens between GB-NECs and GB-ADCs, p value < 0.05 by Student's t test.

Molecular characteristics of GB-NECs

ADC patients. A total of 59 cancer-related genes were found to be mutated in the six GB-NEC cases, while 13 GB-ADC cases exhibited mutations in 60 cancer-related genes (Fig. 2A). Notably, the tumor suppressor genes *TP53* and *RBI* displayed the highest mutation frequency, both at 100% (6/6), in GB-NECs. This was followed by *SMAD4* (50%, 3/6), *GNAS* (50%, 3/6), and Rapamycin-insensitive companion of mammalian target of rapamycin (*RICTOR*, 33%, 2/6). Most mutations in *TP53*, *RBI*, and *SMAD4* led to functional loss. *TP53* mutations comprised copy number loss, nonsense

mutations in exons 5 and 9, frameshift mutations in exon 6, missense mutations in exon 2 and 10, and splice site mutations in exon 10. *RBI* mutations included initiator codon loss, frameshift mutations in exons 8 and 18, nonsense mutations in exons 12 and 14, missense mutations in exon 16, and splice site mutations in intron 5. Notably, cases 1, 2, and 4 of GB-NECs exhibited two different types of *TP53* mutations simultaneously, while case 4 showed two different types of *RBI* mutation. *SMAD4* mutations encompassed copy number loss (2/3) and a nonsense mutation (1/3). In contrast, mutations in

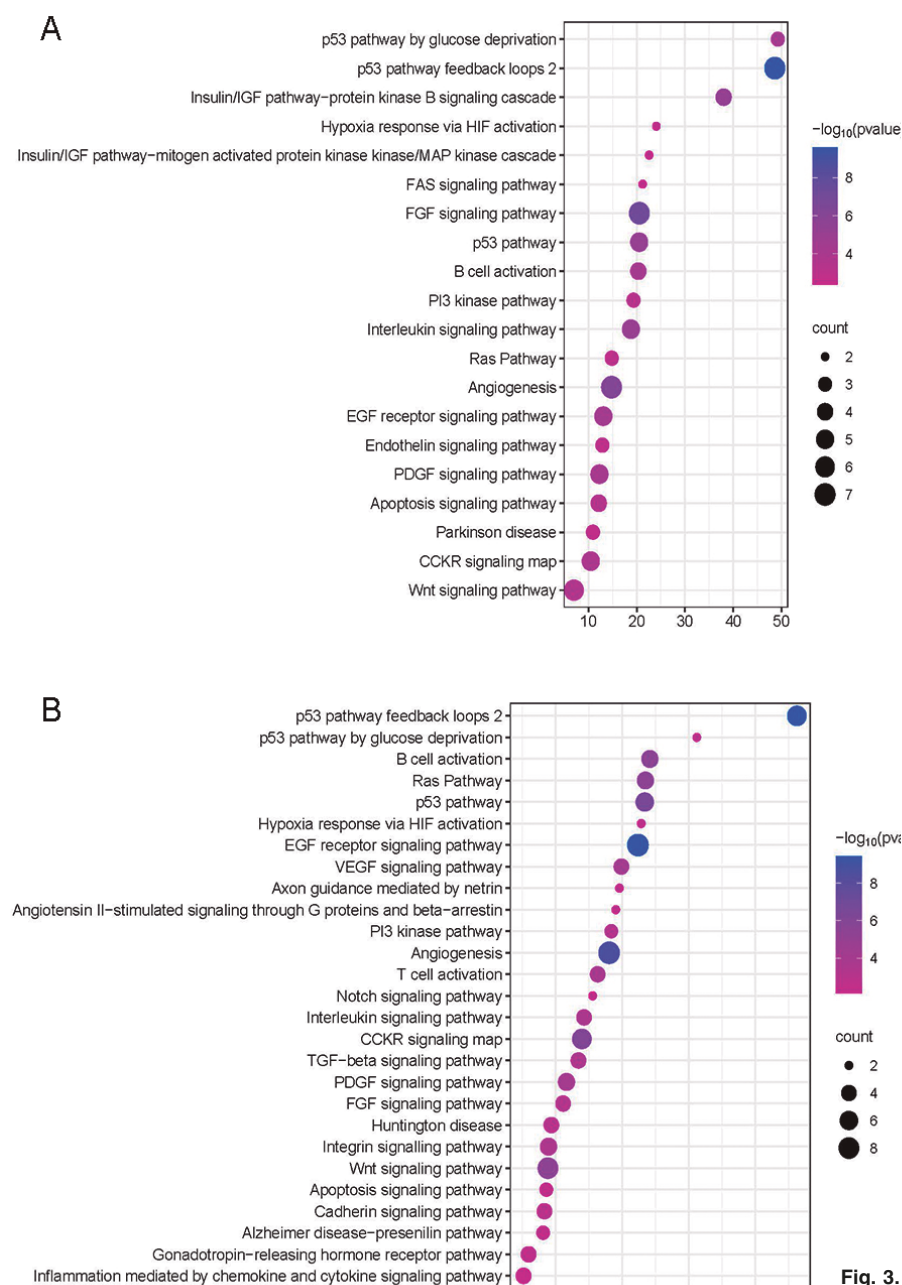


Fig. 3. Pathway enrichment analyses of mutant genes in GB-NECs (A) and GB-ADCs (B).

GNAS and *RICTOR* were predominantly gain-of-function mutations, including copy number amplification and missense mutations (Fig. 2A).

In GB-ADC samples, the most frequently mutated gene was also *TP53* (69%, 9/13), followed by *ARID1A* (31%, 4/13), *CTNNB1* (23%, 3/13), *KRAS* (23%, 3/13), *SMAD4* (23%, 3/13), *ERBB3* (15%, 2/13), *CDKN2A* (15%, 2/13), *ARID2* (15%, 2/13), *EPHA2* (15%, 2/13), and *NF1* (15%, 2/13) (Fig. 2A).

Comparing the distinct genetic mutations between GB-NECs and GB-ADCs, *RBI* (100%, 6/6), *GNAS* (50%, 3/6), and *RICTOR* (33%, 2/6) were mutations specific to GB-NECs (Fig. 2C), while mutations in *ARID1A* (31%, 4/13), *CTNNB1* (23%, 3/13), *ERBB3* (15%, 2/13), *CDKN2A* (15%, 2/13), *EPHA2* (15%, 2/13), and *NF1* (15%, 2/13) were only found in GB-ADCs (Fig. 2D). *TP53* (79%, 15/19), *SMAD4* (32%, 6/19), *KRAS* (21%, 4/19), *ARID2* (16%, 3/19), *APC* (11%, 2/19), *BRCA1* (11%, 2/19), *BTk* (11%, 2/19), *MYC* (11%, 2/19), *PIK3CA* (11%, 2/19), and *RET* (11%, 2/19) were mutated in both GB-NECs and GB-ADCs (Fig. 2B). Notably, the major *P53* mutation type in GB-ADCs was a missense mutation (6/9, 66.7%), and mutations mainly occurred in exon 8 (7/9, 77.78%), whereas in GB-NECs, *TP53* mutations were mainly nonsense mutations or frameshifts (5/6, 83.3%), sporadically distributed in exons 5, 6, 8, and 9. Pathway enrichment analysis showed that mutant genes in GB-NECs and GB-ADCs were mostly enriched in the P53, angiogenesis, PI3K, Ras, and Wnt pathway (Fig. 3).

As previously reported, TMB results obtained from CGP are highly correlated with whole exon sequencing (WES). (Sholl et al., 2020) One GB-NEC patient and three GB-ADC patients displayed high TMB. There was no significant difference in TMB between GB-NEC and GB-ADC patients ($p=0.864$) (Fig. 1E). The microsatellite states of six GB-NECs and 13 GB-ADCs obtained from NGS analysis were all MSS, consistent with observations from the MSI PCR assay and IHC

expression of MMR protein.

Consistency of p53 and Rb IHC with their genetic mutations

The protein levels of p53 and Rb were further assessed in the six GB-NECs tissue samples by IHC. Four cases with nonsense mutation/frameshift mutation/copy number loss in exons 5, 6, and 8 exhibited absent expression of p53. Case 2 missense/splice site mutation in exon 10 and Case 3 with a nonsense mutation in exon 9 showed the abnormal cytoplasmic expression pattern characterized by diffuse cytoplasmic staining with variable and weaker than nuclear staining, both patterns indicated a *TP53* mutation status at the molecular level (Singh et al., 2020; Rabban et al., 2021; Vermij et al., 2022) (Fig. 4). Regarding Rb IHC, five cases with frameshift mutation/nonsense mutation/initiator codon loss in different exons showed negative expression, while case 5 with an *RBI* splice site mutation in intron 5 showed weak nuclear expression, differing from the strong nuclear expression of wild-type Rb (Febres-Aldana et al., 2022) (Fig. 4). Therefore, IHC assessment of p53 and Rb demonstrated high consistency with *TP53* and *RBI* mutations at the molecular level.

Clinical outcome in GB-NECs

Follow-up data were available for the six GB-NEC and seven GB-ADC patients. The median overall survival time for patients with GB-NECs was 16 months, whereas it was 31 months for those with GB-ADCs (Table 2). The overall survival rate among patients with GB-NECs displayed a trend towards poorer outcomes compared with those with GB-ADCs. However, the statistical analysis did not reveal a significant difference between the two groups ($pP=0.119$) (Fig. 5).

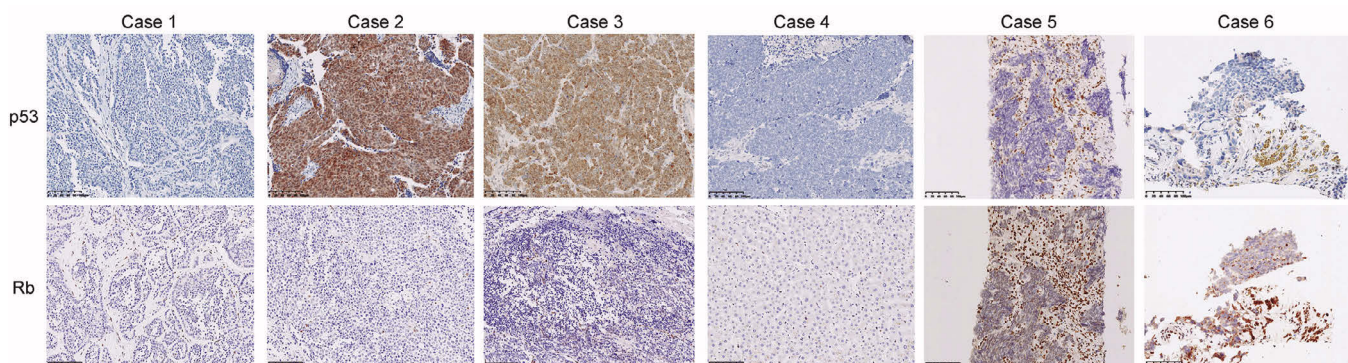


Fig. 4. Immunohistochemical analyses of p53 and Rb in six GB-NECs cases. Case 1, 4-6: Negative expression of p53. Case 2, 3: Abnormal cytoplasmic expression of p53, diffuse cytoplasmic staining with variable and weaker than nuclear staining. Case 1-4, 6: Negative expression of Rb. Case 5: Weakly positive expression of Rb. Scale bar: 100 μ m.

Discussion

Primary neuroendocrine carcinomas of the gallbladder are rare yet highly malignant. Given the low incidence rate of GB-NECs, research into the molecular mechanism underlying their pathogenesis remains limited. Our study attempted to elucidate clinicopathologic and molecular characteristics of neuroendocrine carcinomas in gallbladder based on the analysis of GB-NEC and GB-ADC patients, which was conducive to a deeper understanding of the molecular pathological features of GB-NECs.

In line with trends observed in other gallbladder cancers (Wistuba and Gazdar, 2004; Sahnane et al., 2015; Baiu and Visser, 2018), a significant prevalence of older females was noted among GB-NEC patients (all six were female, mean age of 62 years). Abdominal pain and gallstones (Yan et al., 2020; Zhang et al., 2021) were common clinical symptoms in GB-NEC patients. In our study, SCNEC was the primary pathological subtype, accounting for 66.67% (4/6). The overall survival (OS) of GB-NEC patients appeared worse than that of GB-ADC, although statistical significance was not attained. This finding aligns with some previous reports (Yan et al., 2020; Cai et al., 2022). The main treatment for gallbladder cancer involves surgical resection and cytotoxic chemotherapy (Wang et al., 2022b; Wu et al., 2023). The Ki67 index of six GB-NEC cases in our report ranged from 70% to 95%, which was a predictive marker for platinum-based chemotherapy (Janson et al., 2021; Ooki et al., 2023). Currently, combined treatment with immune checkpoint inhibitors or targeted therapy in GB-NECs has limited evidence and requires further investigation (Hussain et al., 2019; Chorath et al., 2020; Chu et al., 2021).

Our study did not observe microsatellite instability (MSI) in GB-NECs nor GB-ADC patients, with a high concordance between immunohistochemical expression of MMR proteins and the MSI PCR assay. In line with our findings, a previous study reported that the MSI phenotype was frequently observed in gastroenteropancreatic neuroendocrine carcinomas but not in GB-

NECs (Sahnane et al., 2015). However, Li et al. reported a GB-SCNEC case with genome-wide MSI in both the primary and metastatic GB-SCNEC tissue (Li et al., 2017). Giraldo et al. found that out of 233 GBC patients, six tumors showed high MSI (Giraldo et al., 2022). We acknowledge that this study has a limitation of small sample size, therefore the results in this and prior studies suggest that the incidence of MSI is relatively low in GBC patients.

We identified 59 and 60 gene mutations in GB-NECs and GB-ADCs, respectively. *TP53* and *RBI* exhibited high mutation rates in GB-NEC patients (100% mutation in *TP53* and *RB1*), contrasting with GB-ADCs (69% mutation in *TP53* and 0% in *RB1*). Concurrent *RB1/TP53* mutations emerged as a significant molecular pathological feature of GB-NECs. Supporting our findings, Lee et al. observed the loss of Rb1 expression in 74% (25/34) of GB-NEC cases (Lee and Sung, 2020). Additionally, Liu et al. reported a high mutation frequency (27%) of *RB1* in GB-NECs, contrasting with its absence in GB-ADCs (Liu et al., 2021). Co-mutations of *RB1/TP53* have been observed in various cancer types, particularly in small cell carcinomas, neuroendocrine carcinomas, and sarcomas (Uccella et al., 2021; Cai and Wu, 2022; Rindi et al., 2022; Ooki et al., 2023), possibly affecting the self-renewal program in neuroendocrine cells with stem cell potential (Ouadah et al., 2019), and co-mutation of these two tumor suppressor genes may collaborate to disrupt cell fate control (Yamada and Beltran, 2021). Several preclinical studies have now supported combined *TP53* and *RB1* deficiency as key facilitators of the neuroendocrine-like phenotype (Ku et al., 2017; Mu et al., 2017; Kaur et al., 2020). The involvement of *SOX2* downstream of *RB1* and *TP53*, along with *SOX2* methylation, suggests a role in reverting cells to a stem-like state before differentiating into a neuroendocrine lineage (Mu et al., 2017; Ooki et al., 2023). However, further investigation is required to elucidate the mechanism underlying *RB1/TP53* co-mutation in the malignant transformation of GB-NECs.

Our study also highlighted the consistency between the IHC assay of p53 and Rb with their genetic mutations, as identified by NGS. Abnormal p53 IHC expression patterns, including overexpression, negative and cytoplasmic expression, correlated with specific *TP53* genomic alterations (Singh et al., 2020; Rabban et al., 2021; Vermij et al., 2022). In our study, nonsense mutation/frameshift mutation in exons 5, 6, and 8 were associated with absent expression of p53. While the nonsense mutation in exon 9 [c.991C> T (p. Q331*)] located in the *TP53* tetramerization domain (amino acids 325 to 356) correlated with the cytoplasmic expression pattern. A splice site mutation and a missense mutation in exon 10 of *TP53* also exhibited the cytoplasmic expression pattern. Similarly, *RB1* gene mutations were associated with varied levels of nuclear Rb expression. Frameshift mutation/nonsense mutation/ initiator codon loss in exons of *RB1* resulted in a total loss of Rb

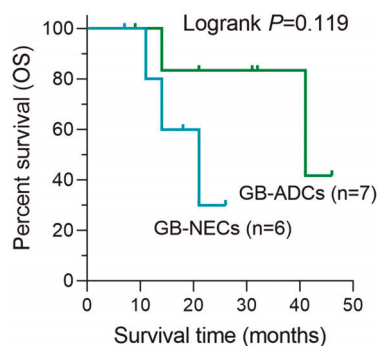


Fig. 5. Kaplan-Meier curves displaying the difference of overall survival between GB-NECs and GB-ADCs. No significant difference was found between two groups.

expression, while a splice-site mutation in intron 5 (c.540-2A>G) of *RBI* exhibited low levels of nuclear expression. The *RBI* gene is a 178 kb large gene containing 29 exons, and the introns account for 99% of the total gene length. *RBI* genomic alterations are mainly enriched in intronic splice-site mutations and structural variants (Jung et al., 2021). A previous study analyzing 10 small cell lung cancer cases with expressed/mutated *Rb* harbored predominantly splice-site mutations in *RBI* (70%) (Febres-Aldana et al., 2022). Hence, the IHC of p53 provides an effective complement to targeted NGS for determining the functional status of p53 and *Rb* in clinical practice.

Moreover, other frequently mutated genes in GB-NECs included *SMAD4* (50%), *GNAS* (50%), and *RICTOR* (33%). *SMAD4* is a tumor suppressor involved in the TGF- β /SMAD4 signaling pathway and inhibits tumor proliferation mainly by inducing cell cycle arrest and apoptosis. In our study, *SMAD4* exhibited loss-of-function mutations in 50% of GB-NECs and 23% of GB-ADCs. Deletions or mutations in *SMAD4* have been implicated in pancreatic cancer, cholangiocarcinoma, and colorectal cancer (Zhao et al., 2018). This suggests a potential tumor-suppressive role for *SMAD4* in both GB-NECs and GB-ADCs. The *GNAS* gene encodes the α -subunit of a stimulatory G-protein (*Gas*), which activates adenylate cyclase, thereby increasing cyclic adenosine monophosphate (cAMP) levels, leading to cancer-promoting activities (Ohtsuka et al., 2019). Initially, genetic alterations in G proteins were primarily detected in endocrine tumors, *GNAS* mutations promoted hyperplasia of endocrine cells in human thyroid and pituitary tumors (O'Hayre et al., 2013). Then *GNAS* activating mutations particularly in codons R201C and R201H are frequently detected in colorectal cancers and intraductal papillary neoplasms of the pancreas and biliary tract (O'Hayre et al., 2013; Ohtsuka et al., 2019; Afolabi et al., 2022). In our study, *GNAS* amplification mutations were detected in two GB-NEC cases, and one case exhibited a missense mutation, c.1048G>C (p. E350Q). This suggests a potential role for *GNAS* as an active oncogene in GB-NECs. *RICTOR*, critical in the PI3K/AKT/mTOR pathway and cell growth, was amplified in one GB-NEC case. Co-mutation of *RICTOR* [c.2062C>G (p. L688V)], *PIK3CA* [c.1624G>A (p. E542K)], and *AKT2* (amplification) was observed in another GB-NEC case. A high *RICTOR* expression was associated with low OS in tumors such as colorectal cancer, ovarian cancer, lung adenocarcinoma (Sun et al., 2023). Genetic alteration in *RICTOR* has also been noted in LCNEC of the lung (Miyoshi et al., 2017) and SCNEC of the cervix (Madžarac et al., 2023). The amplification of *RICTOR* or co-mutation of *RICTOR* with PI3K/AKT/mTOR pathway molecules might contribute to tumor activation in GB-NECs, warranting further investigation.

The *KRAS* G12C mutation was detected in one case each of GB-NECs and GB-ADCs. This mutation has been reported in other neuroendocrine tumors (Wang et

al., 2022a). Targeted therapy for *KRAS* G12C mutations has shown remarkable progress in recent years, suggesting the feasibility of adjuvant therapy combined with targeted therapy in GB-NET patients. In our study, mutations in *ERBB2/3/4* were only found in three cases of GB-ADCs (23%), consistent with the research results of Li et al. (2014). The ErbB signaling pathway may be extensively mutated in GB-ADCs.

Conclusions

In conclusion, both GB-NECs and GB-ADCs were identified as microsatellite stable. Despite a limited number of GB-NEC cases, distinct somatic mutation profiles were observed between these subtypes. The presence of *RBI/TP53* co-mutations may indicate a neuroendocrine tendency for GB-NECs. Additionally, global loss or abnormal expression of p53/*Rb* by IHC may serve as an ancillary marker for the pathologic diagnosis of GB-NECs. The frequently mutated genes identified in our study were similar to those of the existing literature. The results of our investigation will contribute to a deeper understanding of the molecular pathological characteristics of GB-NECs.

Acknowledgements. We thank Dr. Luo Danju and Dr. Fan Jun from Union Hospital Affiliated with Huazhong University of Science and Technology Wuhan China for their valuable suggestions on our article.

Institutional Review Board Statement. The study was conducted in accordance with the Declaration of Helsinki, and approved by the Institutional Ethics Committee of the First Affiliated Hospital, Zhejiang University School of Medicine (protocol code: 2023-0579, August 4th, 2023).

Author Contributions. H.T. and Y.Z. performed the study concept and design; H.T., X. J., L.Z., C.R., X.L. and Y.Z. developed the methodology, statistical analysis, writing, review, and revision of the paper; H.T., L.X., X.W., F.G. and H.L. provided acquisition, analysis, and interpretation of data. All authors read and approved the final paper.

Funding. This work was supported by the Natural Science Foundation of Zhejiang Province (LY22H090021), Innovative Talent Support Program of Zhejiang Medical and Health Research Project (Zhejiang province) (2020RC056), Yangzhou Science and Technology Planning (YZ2023100), Lv Yang Jin Feng Talent Program of Yangzhou (LYJF00039), Yangzhou Science and Technology Planning (YZ2020076).

Data Availability Statement. All data accessed and analyzed in this study are available in the article and its Supplementary Materials.

References

- Afolabi H.A., Salleh S.M., Zakaria Z., Ch'ng E.S., Mohd Nafi S.N., Abdul Aziz A.A.B., Irekeola A.A., Wada Y. and Al-Mhanna S.B. (2022). A *GNAS* gene mutation's independent expression in the growth of colorectal cancer: A systematic review and meta-analysis. *Cancers* 14, 5480.
- Baiu I. and Visser B. (2018). Gallbladder cancer. *JAMA* 320, 1294.
- Bray F., Ferlay J., Soerjomataram I., Siegel R.L., Torre L.A. and Jemal A. (2018). Global cancer statistics 2018: GLOBOCAN estimates of

Molecular characteristics of GB-NECs

- incidence and mortality worldwide for 36 cancers in 185 countries. *CA Cancer J. Clin.* 68, 394-424.
- Byrd D.R., Carducci M.A., Compton C.C., Fritz A.G. and Greene F.L. (2017). *AJCC Cancer Staging Manual*. 8th ed. Springer. New York.
- Cai X. and Wu S. (2022). Gallbladder neuroendocrine carcinoma diagnosis, treatment and prognosis based on the SEER database: A literature review. *World J. Clin. Cases* 10, 8212-8223.
- Cai L., DeBerardinis R.J., Xiao G., Minna J.D. and Xie Y. (2022). A pan-cancer assessment of RB1/TP53 co-mutations. *Cancers* 14, 4199.
- Chorath J., Placencio-Hickok V.R., Guan M., Nissen N., Kamrava M., Klempner S.J., Nassir Y., Hendifar A. and Gong J. (2020). Durable response to carboplatin, etoposide, nivolumab, and ipilimumab in metastatic high-grade neuroendocrine carcinoma of the gallbladder. *Pancreas* 49, e19-e20.
- Chu H., Shi Y., Liu J., Huang D., Zhang J. and Dou C. (2021). Update in clinical management for gallbladder neuroendocrine carcinoma. *Medicine* 100, e25449.
- Febres-Aldana C.A., Chang J.C., Ptashkin R., Wang Y., Gedvilaite E., Baine M.K., Travis W.D., Ventura K., Bodd F., Yu H.A., Quintanal-Villalonga A., Lai W.V., Egger J.V., Offin M., Ladanyi M., Rudin C.M. and Rekhman N. (2022). Rb tumor suppressor in small cell lung cancer: Combined genomic and IHC analysis with a description of a distinct Rb-proficient subset. *Clin. Cancer Res.* 28, 4702-4713.
- Giraldo N.A., Drill E., Satravada B.A., Dika I.E., Brannon A.R., Dermawan J., Mohanty A., Ozcan K., Chakravarty D., Benayed R., Vakiani E., Abou-Alfa G.K., Kundra R., Schultz N., Li B.T., Berger M.F., Harding J.J., Ladanyi M., O'Reilly E.M., Jarnagin W., Vanderbilt C., Basturk O. and Arcila M.E. (2022). Comprehensive molecular characterization of gallbladder carcinoma and potential targets for intervention. *Clin. Cancer Res.* 28, 5359-5367.
- Gustafsson B.I., Kidd M. and Modlin I.M. (2008). Neuroendocrine tumors of the diffuse neuroendocrine system. *Curr. Opin. Oncol.* 20, 1-12.
- Hundal R. and Shaffer E.A. (2014). Gallbladder cancer: epidemiology and outcome. *Clin. Epidemiol.* 6, 99-109.
- Hussain I., Sarvepalli D., Zafar H., Jehanzeb S. and Ullah W. (2019). Neuroendocrine tumor: A rare, aggressive tumor of the gallbladder. *Cureus* 11, e5571.
- Janson E.T., Knigge U., Dam G., Federspiel B., Grønbaek H., Stålberg P., Langer S.W., Kjaer A., Arola J., Schalin-Jääntti C., Sundin A., Welin S., Thiis-Evensen E. and Sorbye H. (2021). Nordic guidelines 2021 for diagnosis and treatment of gastroenteropancreatic neuroendocrine neoplasms. *Acta Oncol.* 60, 931-941.
- Jung H., Lee K.S. and Choi J.K. (2021). Comprehensive characterisation of intronic mis-splicing mutations in human cancers. *Oncogene* 40, 1347-1361.
- Kaur H., Samarska I., Lu J., Faisal F., Maughan B.L., Murali S., Asrani K., Alshalalfa M., Antonarakis E.S., Epstein J.I., Joshi C.E., Schaeffer E.M., Mosquera J.M. and Lotan T.L. (2020). Neuroendocrine differentiation in usual-type prostatic adenocarcinoma: Molecular characterization and clinical significance. *Prostate* 80, 1012-1023.
- Ku S.Y., Rosario S., Wang Y., Mu P., Seshadri M., Goodrich Z.W., Goodrich M.M., Labbé D.P., Gomez E.C., Wang J., Long H.W., Xu B., Brown M., Loda M., Sawyers C.L., Ellis L. and Goodrich D.W. (2017). Rb1 and Trp53 cooperate to suppress prostate cancer lineage plasticity, metastasis, and antiandrogen resistance. *Science* 355, 78-83.
- La Rosa S. and Uccella S. (2021). Classification of neuroendocrine neoplasms: Lights and shadows. *Rev. Endocr. Metab. Disord.* 22, 527-538.
- Lee S.M. and Sung C.O. (2020). Neuroendocrine carcinomas of the gallbladder: A clinicopathologic and immunohistochemical analysis of 34 resected cases. *Am. J. Surg. Pathol.* 44, 1308-1321.
- Li M., Zhang Z., Li X., Ye J., Wu X., Tan Z., Liu C., Shen B., Wang X.A., Wu W., Zhou D., Zhang D., Wang T., Liu B., Qu K., Ding Q., Weng H., Ding Q., Mu J., Shu Y., Bao R., Cao Y., Chen P., Liu T., Jiang L., Hu Y., Dong P., Gu J., Lu W., Shi W., Lu J., Gong W., Tang Z., Zhang Y., Wang X., Chin Y.E., Weng X., Zhang H., Tang W., Zheng Y., He L., Wang H., Liu Y. and Liu Y. (2014). Whole-exome and targeted gene sequencing of gallbladder carcinoma identifies recurrent mutations in the ErbB pathway. *Nat. Genet.* 46, 872-876.
- Li M., Liu F., Zhang Y., Wu X., Wu W., Wang X.A., Zhao S., Liu S., Liang H., Zhang F., Ma Q., Xiang S., Li H., Jiang L., Hu Y., Gong W., Zhang Y., Ma T., Zhang K., Liu Y. and Liu Y. (2017). Whole-genome sequencing reveals the mutational landscape of metastatic small-cell gallbladder neuroendocrine carcinoma (GB-SCNEC). *Cancer Lett.* 391, 20-27.
- Liu F., Li Y., Ying D., Qiu S., He Y., Li M., Liu Y., Zhang Y., Zhu Q., Hu Y., Liu L., Li G., Pan W., Jin W., Mu J., Cao Y. and Liu Y. (2021). Whole-exome mutational landscape of neuroendocrine carcinomas of the gallbladder. *Signal Transduct. Target. Ther.* 6, 55.
- Madžarac V., Culej D., Mužinić D., Zovko G., Fenzl V. and Duić Ž. (2023). Small-cell neuroendocrine carcinoma of the cervix associated with adenocarcinoma *in situ*: A case report with analysis of molecular abnormalities. *Neuro. Endocrinol. Lett.* 44, 332-335.
- Miyoshi T., Umemura S., Matsumura Y., Mimaki S., Tada S., Makinoshima H., Ishii G., Udagawa H., Matsumoto S., Yoh K., Niho S., Ohmatsu H., Aokage K., Hishida T., Yoshida J., Nagai K., Goto K., Tsuboi M. and Tsuchihara K. (2017). Genomic profiling of large-cell neuroendocrine carcinoma of the lung. *Clin. Cancer Res.* 23, 757-765.
- Mu P., Zhang Z., Benelli M., Karthaus W.R., Hoover E., Chen C.C., Wongvipat J., Ku S.Y., Gao D., Cao Z., Shah N., Adams E.J., Abida W., Watson P.A., Prandi D., Huang C.H., de Stanchina E., Lowe S.W., Ellis L., Beltran H., Rubin M.A., Goodrich D.W., Demichelis F. and Sawyers C.L. (2017). SOX2 promotes lineage plasticity and antiandrogen resistance in TP53- and RB1-deficient prostate cancer. *Science* 355, 84-88.
- O'Hayre M., Vázquez-Prado J., Kufareva I., Stawiski E.W., Handel T.M., Seshagiri S. and Gutkind J.S. (2013). The emerging mutational landscape of G proteins and G-protein-coupled receptors in cancer. *Nat. Rev. Cancer* 13, 412-424.
- Ohtsuka T., Tomosugi T., Kimura R., Nakamura S., Miyasaka Y., Nakata K., Mori Y., Morita M., Torata N., Shindo K., Ohuchida K. and Nakamura M. (2019). Clinical assessment of the GNAS mutation status in patients with intraductal papillary mucinous neoplasm of the pancreas. *Surg. Today* 49, 887-893.
- Ooki A., Osumi H., Fukuda K. and Yamaguchi K. (2023). Potent molecular-targeted therapies for gastro-entero-pancreatic neuroendocrine carcinoma. *Cancer Metastasis Rev.* 42, 1021-1054.
- Ouahad Y., Rojas E.R., Riordan D.P., Capostagno S., Kuo C.S. and Krasnow M.A. (2019). Rare pulmonary neuroendocrine cells are stem cells regulated by Rb, p53, and Notch. *Cell* 179, 403-416.e423.
- Rabban J.T., Garg K., Ladwig N.R., Zaloudek C.J. and Devine W.P. (2021). Cytoplasmic pattern p53 immunoreactivity in pelvic and endometrial carcinomas with TP53 mutation involving nuclear localization domains. *Am. J. Surg. Pathol.* 45, 1441-1451.

- Rindi G., Mete O., Uccella S., Basturk O., La Rosa S., Brosens L.A.A., Ezzat S., de Herder W.W., Klimstra D.S., Papotti M. and Asa S.L. (2022). Overview of the 2022 WHO classification of neuroendocrine neoplasms. *Endocr. Pathol.* 33, 115-154.
- Roa J.C., Basturk O. and Adsay V. (2021). Dysplasia and carcinoma of the gallbladder: pathological evaluation, sampling, differential diagnosis and clinical implications. *Histopathology* 79, 2-19.
- Sahnane N., Furlan D., Monti M., Romualdi C., Vanoli A., Vicari E., Solcia E., Capella C., Sessa F. and La Rosa S. (2015). Microsatellite unstable gastrointestinal neuroendocrine carcinomas: a new clinicopathologic entity. *Endocr. Relat. Cancer* 22, 35-45.
- Sholl L.M., Hirsch F.R., Hwang D., Botling J., Lopez-Rios F., Bubendorf L., Mino-Kenudson M., Roden A.C., Beasley M.B., Borczuk A., Brambilla E., Chen G., Chou T.Y., Chung J.H., Cooper W.A., Dacic S., Lantuejoul S., Jain D., Lin D., Minami Y., Moreira A., Nicholson A.G., Noguchi M., Papotti M., Pelosi G., Poleri C., Rehkhtman N., Tsao M.S., Thunnissen E., Travis W., Yatabe Y., Yoshida A., Daigneault J.B., Zehir A., Peters S., Wistuba, II, Kerr K.M. and Longshore J.W. (2020). The promises and challenges of tumor mutation burden as an immunotherapy biomarker: A perspective from the international association for the study of lung cancer pathology committee. *J. Thorac. Oncol.* 15, 1409-1424.
- Singh N., Piskorz A.M., Bosse T., Jimenez-Linan M., Rous B., Brenton J.D., Gilks C.B. and Köbel M. (2020). p53 immunohistochemistry is an accurate surrogate for TP53 mutational analysis in endometrial carcinoma biopsies. *J. Pathol.* 250, 336-345.
- Sun Y., Li R., Nong B., Songyang Z., Wang X., Ma W. and Zhou Q. (2023). A comprehensive pan-cancer analysis of the potential biological functions and prognosis values of RICTOR. *Genes* 14, 1280.
- Uccella S., La Rosa S., Metovic J., Marchiori D., Scoazec J.Y., Volante M., Mete O. and Papotti M. (2021). Genomics of high-grade neuroendocrine neoplasms: Well-Differentiated neuroendocrine tumor with high-grade features (G3 NET) and neuroendocrine carcinomas (NEC) of various anatomic sites. *Endocr. Pathol.* 32, 192-210.
- Vermij L., León-Castillo A., Singh N., Powell M.E., Edmondson R.J., Genestie C., Khaw P., Pyman J., McLachlin C.M., Ghatage P., de Boer S.M., Nijman H.W., Smit V.T.H.B.M., Crosbie E.J., Leary A., Creutzberg C.L., Horeweg N., Bosse T., Horeweg N., de Boer S.M., Creutzberg C.L., Bosse T., Smit V.T.H.B.M., Kroep J., Nout R.A., Nijman H.W., de Bruyn M., Powell M.E., Singh N., Kitchener H.C., Crosbie E., Edmondson R., Church D.N., Leary A., Mileshekin L., Pollock P.M. and MacKay H. (2022). p53 immunohistochemistry in endometrial cancer: clinical and molecular correlates in the PORTEC-3 trial. *Mod. Pathol.* 35, 1475-1483.
- Wang S., Li Q., Ma P., Fang Y., Yu Y., Jiang N., Miao H., Tang Q., Yang Y., Xing S., Chen R., Yi X. and Li N. (2022a). KRAS mutation in rare tumors: A landscape analysis of 3453 chinese patients. *Front. Mol. Biosci.* 9, 831382.
- Wang W., Yang C.X., Yu X.Z., Zhang S.L., Wang J. and Wang J. (2022b). Clinicopathological characteristics and prognostic factors of patients with primary gallbladder neuroendocrine carcinomas. *J. Dig. Dis.* 23, 166-173.
- Wistuba I.I. and Gazdar A.F. (2004). Gallbladder cancer: lessons from a rare tumour. *Nat. Rev. Cancer* 4, 695-706.
- Wu X., Li B., Hong T., Liu W., He X. and Zheng C. (2023). Neuroendocrine neoplasm of the gallbladder: Clinical features, surgical efficacy, and prognosis. *Cancer Med.* 12, 11344-11350.
- Yamada Y. and Beltran H. (2021). Clinical and biological features of neuroendocrine prostate cancer. *Curr. Oncol. Rep.* 23, 15.
- Yan S., Wang Y., Chen X., Zhang Y., Huang Z., Zhao J., Zhou J., Li Z., Bi X., Luo Z., Cai J. and Zhao H. (2020). Clinical analysis of 15 cases of gallbladder neuroendocrine carcinoma and comparison with gallbladder adenocarcinoma using a propensity score matching. *Cancer Manag. Res.* 12, 1437-1446.
- Yao J.C., Hassan M., Phan A., Dagohoy C., Leary C., Mares J.E., Abdalla E.K., Fleming J.B., Vauthey J.N., Rashid A. and Evans D.B. (2008). One hundred years after "carcinoid": epidemiology of and prognostic factors for neuroendocrine tumors in 35,825 cases in the United States. *J. Clin. Oncol.* 26, 3063-3072.
- Zhang Z., Guo T., Huang X., Xie P., Wang L. and Yu Y. (2021). Age-specific clinicopathological characteristics and prognostic analysis of neuroendocrine carcinomas of the gallbladder. *Cancer Med.* 11, 641-653.
- Zhao M., Mishra L. and Deng C.-X. (2018). The role of TGF- β /SMAD4 signaling in cancer. *Int. J. Biol. Sci.* 14, 111-123.
- Zhu L., Huang Y., Fang X., Liu C., Deng W., Zhong C., Xu J., Xu D. and Yuan Y. (2018). A novel and reliable method to detect microsatellite instability in colorectal cancer by next-generation sequencing. *J. Mol. Diagn.* 20, 225-231.